The stellate vascular smooth muscle cell phenotype is induced by IL-1β via the secretion of PGE2 and subsequent cAMP-dependent protein kinase A activation

Karl Blirando, Régis Blaise, Natalia Gorodnaya, Clotilde Rouxel, Olivier Meilhac, Pierre Vincent, Isabelle Limon

The stellate vascular smooth muscle cell phenotype is induced by IL-1β *via* the secretion of PGE_2 and subsequent cAMP-dependent protein kinase A activation

Karl Blirando[1], Regis Blaise[1], Natalia Gorodnaya[1], Clotilde Rouxel[1], Olivier Meilhac[2], Pierre Vincent[1] and Isabelle Limon[1*].

1. Sorbonne Universités, UPMC Univ Paris 06, CNRS, UMR 8256 B2A, IBPS, F-75005, Paris, France.
2. Inserm U1188 Diabète Athérothrombose Thérapies Réunion Océan Indien (DéTROI) CYROI, 2, rue Maxime Rivière 97490 Sainte Clotilde, La Réunion.

*: Corresponding author: 7, quai St Bernard, Bat A 5ème étage, 75005 Paris, France.
Tel.: 33144273716; e-mail: isabelle.limon@upmc.fr.

Abstract

Atherosclerosis development is associated with morphological changes to intimal cells, leading to a stellate cell phenotype. In this study, we aimed to determine whether and how key pro-atherogenic cytokines present in atherosclerotic plaques (IL-1β, TNFα and IFNγ) could induce this phenotype, as these molecules are known to trigger the transdifferentiation of vascular smooth muscle cells (VSMCs). We found that, IL-1β was the only major inflammatory mediator tested capable of inducing a stellate morphology in VSMCs. This finding was confirmed by staining for F-actin and vinculin at focal adhesions, as these two markers were disrupted only by IL-1β. We then investigated the possible association of this IL-1β-dependent change in morphology with an increase in intracellular cAMP concentration ([cAMP]), using the FRET-based biosensor for cAMP $^{T}Epac^{VV}$**.** Experiments in the presence of IL-1β or medium conditioned by IL-1β-treated VSMCs and pharmacological tools demonstrated that the long-term increase in intracellular cAMP concentration was induced by the secretion of an autocrine/paracrine mediator, prostaglandin E_2 (PGE_2), acting through the EP4 receptor. Finally, by knocking down the expression of the regulatory subunit PKAR1α, thereby reproducing the effects of IL-1β and PGE_2 on VSMCs, we demonstrated the contribution of PKA activity to the observed behavior of VSMCs.

Keywords: Vascular smooth muscle cells, IL-1β, PGE_2, cAMP, PKA, stellate cell morphology.

List of abbreviations:

6-BNZ: N^6- benzoyladenosine- 3', 5'- cyclic monophosphate

8-pCPT-O-Me-cAMP: 8-(4-chlorophenylthio)-2'-O-methyladenosine-3', 5'-cyclic monophosphate sodium salt

ApoE: apolipoprotein E

cAMP: cyclic adenosine monophosphate

CCL3 or MIP-1α: chemokine (C-C motif) ligand 3

CCL5 or RANTES: chemokine (C-C motif) ligand 5

CCL18 or PARC: chemokine (C-C motif) ligand 18

CFP: cyan fluorescent protein

COX-2: cyclooxygenase-2

CX3CL1 or fraktalkin: chemokine (C-X3-C motif) ligand 1

CXCL1: chemokine (C-X-C motif) ligand 1

CXCL10: chemokine (C-X-C motif) ligand 10

CXCL2: chemokine (C-X-C motif) ligand 2

CXCL3: chemokine (C-X-C motif) ligand 3

CXCL5: chemokine (C-X3-C motif) ligand 5

DAPI: 4',6'-diamidino-2-phenylindole

DMEM: Dulbecco's modified Eagle's medium

Epac: exchange proteins directly activated by cAMP

FRET: fluorescence resonance energy transfer

FSK: forskolin

GM-CSF: granulocyte macrophage colony-stimulating factor

IBMX: isobutyl-L-methylxanthine

IFNγ: interferon γ

IL-1β: interleukin-1β

IL6: Interleukin-6

LDL: low-density lipoproteins

PBS: phosphate-buffered saline

PGE_2: prostaglandin E_2

PKA: protein kinase A

PTGES1: prostaglandin E synthase1

qPCR: quantitative polymerase chain reaction

Rap: Ras-related protein

RhoA: Ras homolog gene family, member A

Rp-8Br-cAMPS: 8- bromoadenosine- 3', 5'- cyclic monophosphorothioate, Rp- isomer

SM-MHC: smooth muscle-myosin heavy chain

SM22: smooth muscle alpha 22

sPLA2a: secreted phospholipase A type IIa

$^{T}Epac^{VV}$: exchange protein directly activated by cAMP between turquoise (T) and venus-venus (VV)

TNFα: tumor necrosis factor α

VEGF: vascular endothelial growth factor

VSMC: vascular smooth muscle cells

YFP: yellow fluorescent protein

1. Introduction

Atherosclerosis is the pathological process underlying most cardiovascular diseases, including acute coronary syndrome, peripheral artery disease and ischemic stroke. It is characterized by chronic inflammation of the arterial wall at sites of blood flow disturbance, leading to the formation of atherosclerotic plaques [**1**]. Atherosclerosis is promoted by hypercholesterolemia, which favors the infiltration of cholesterol-containing LDL into the intima of the vessels [**2**], where it may be oxidized. Parietal monocytes, which differentiate into macrophages [**3**] and vascular smooth muscle cells (VSMCs), which have a macrophage-like phenotype, take up and destroy oxidized LDLs via their scavenger receptors. They then become foam cells, and acquire the ability to secrete several different cytokines, including tumor necrosis factor α (TNFα) and interleukin-1β (IL-1β) [**4**]. Other inflammatory cells, including natural killer cells and lymphocytes, also participate in chronic inflammation by releasing interferon γ (IFNγ), [**5**]. The secretion of these compounds contributes to the expansion of atherosclerotic lesions, notably by inducing medial VSMCs to undergo transdifferentiation, modifying their phenotype.

Actin polymerization is involved in the maintenance of the differentiated/contractile phenotype of VSMCs [**6-8**]. Disruption, defects of actin cytoskeleton protein smooth muscle 22 alpha (SM22 alpha) are associated with pro-inflammatory and chondrogenic changes to the VSMC phenotype, aggravating vascular inflammation and pathological remodeling [**9, 10**]. The transdifferentiated VSMCs also acquire new cellular functions, including roles in migration and proliferation, and these functions are regulated by dynamic actin microfilament rearrangements that may result in changes to cell morphology [**11-13**]. Atherosclerosis development is thus associated with morphological changes to the intimal VSMCs, mostly resulting in the adoption of a stellate form due to the loss of focal adhesions and the disassembly of actin stress fibers. There are very few if any stellate cells in healthy human aortas, but the number of these cells steadily increases as fatty streaks gradually develop into advanced atherosclerotic plaques [**14**]. The role of VSMCs in atherogenesis may have been largely underestimated, because the markers used to identify these cells may not be appropriate **[15**]. Stellate VSMCs were first detected in human aortas, by electron microscopy, in 1986 [**14**]. This phenotype is well known in hepatic fibrosis [**16**], but little is known about the role of stellate VSMCs in atherosclerosis and the potential mediators triggering the change in phenotype from contractile to stellate cells.

We show here that IL-1β was the only inflammatory mediator of those tested (IL-1β, TNFα and IFNγ, all of which are present in plaques) able to trigger the phenotypic transition from contractile to stellate cells in VSMCs. Early studies described an increase in cAMP concentration as the intracellular event leading VSMCs to adopt a stellate phenotype [**17-20**]. We therefore investigated the possible association of the IL-1β-dependent transdifferentiation of VSMCs with the increase in intracellular [cAMP], using a FRET-based biosensor for cAMP (^{T}Epac^{VV}, [**21**])**.** This technique can be used to monitor real-time changes in intracellular [cAMP] in living cells. These experiments showed that the increase in intracellular [cAMP] in response to IL-1β stimulation was due to the secretion of a unique autocrine/paracine mediator, PGE_2. By interacting with the EP4 receptor, PGE_2 stimulates cAMP production, in turn activating PKA and destabilizing the actin cytoskeleton and focal adhesions.

2. Materials and Methods

2.1. Reagents

DMEM, type I collagen from calf skin, L-glutamine, penicillin, streptomycin, fatty acid-free bovine serum albumin, isobutyl-L-methylxanthine (IBMX), FITC-conjugated monoclonal anti-vinculin clone hVIN-1, and monoclonal mouse anti-β-actin clone AC-15, were obtained from Sigma Aldrich, Saint Quentin Fallavier, France. Rabbit anti-hospho PKA substrate antibody (100G7E) was obtained from Cell Signaling, Leiden, the Netherlands. We purchased 8-(4-chlorophenylthio)-2'-o-methyladenosine-3', 5'-cyclic monophosphate sodium salt (8-pCPT-O-Me-cAMP), N6-benzoyladenosine- 3', 5'- cyclic monophosphates (6BNZ-cAMP) and 8- bromoadenosine- 3', 5'- cyclic monophosphorothioate, and Rp- isomer (Rp-8-Br-cAMPS) from BioLog, Bremen, Germany. Forskolin (FSK) was obtained from Tocris Bioscience, Bristol, UK. Fetal calf serum (FCS), FluoroBrite^{TM} DMEM and collagenase were purchased from Gibco BRL, Cergy Pontoise, France. Elastase, and LightCycler-DNA Master Plus SYBR Green were obtained from Roche Diagnostics, Meylan, France. Alexa Fluor® 594-conjugated phalloidin, OPTI–MEM, Fluorobrite DMEM and Lipofectamine® RNAiMAX Reagent were obtained from Invitrogen, Saint Aubin, France. Oligonucleotides were obtained from Eurofins Genomics, Ebersberg, Germany. Recombinant human IL-1β, rat TNFα and IFNγ were obtained from Peprotech, Neuilly-sur-Seine, France. The PGE2 receptor antagonists, L-798 106 (EP3R), SC51322 (EP1R) and ONO AE3208 (EP4R) were obtained from Tocris Bioscience, Bristol, United Kingdom.

2.2. Cell culture

Rats were euthanized by the *i.p.* injection of pentobarbital (300 mg/kg) and VSMCs were isolated as previously described [**22**]. The university ethics committee approved the experiments on rats and all animal procedures conformed to European Directive 2010/63/EU. The VSMC response to IL-1β decreased rapidly with successive cell passages. We therefore performed all experiments on cells that had been subcultured only one to three times. We coated the wells of culture slides with collagen by incubation overnight. The wells were then seeded with cells at a density of 5000 cells/cm^2, in DMEM containing 1g/l glucose, 4 mM L-glutamine, 10% fetal calf serum, 100 U/ml penicillin, 100 µg/ml streptomycin, and the plates were incubated for 96 h, at 37°C, under an atmosphere containing 5% CO_2. The cells were starved by incubation in serum-free DMEM for 7 to 16 h before treatment. We prepared

conditioned medium for FRET experiments, by starving the cells in serum-free Fluorobrite DMEM, to minimize background fluorescence.

2.3. Transfection with a small interfering RNA (siRNA)

VSMCs were grown to about 80% confluence, and were maintained for 2 h in antibiotic-free DMEM containing 1 g/l glucose, 4 mM L-glutamine, 10% FCS. Transfection was then performed by adding 0.25% Lipofectamine and 1 nM siRNA in 12.5 % Opti-MEM and incubating the cells for 24 h. The cells were then starved of serum and treated for 48 h. The siRNAs used were a mixture of 30 different sequences called siPools purchased from Sitools Biotech GmbH (Planegg, Germany) and directed against rat PRKAR1α (NM_013181.1) and rat PRKAR1β (NM_001033679.1).

2.4. Protein extraction and western blot analysis

Cells were washed with ice-cold phosphate-buffered saline (PBS) and scraped into lysis buffer (25 mM Tris–HCl, pH 7.5, 150 mM NaCl, 1% NP40, 1% sodium deoxycholate, 0.1% SDS) supplemented with Halt phosphatase and protease inhibitor cocktail (Pierce, Thermo-Scientific, Villebon sur Yvette, France). Cell lysates were incubated on a rotating wheel for 15 min at 4°C. The lysates were then cleared by centrifugation (13000 x *g* for 15 min at 4°C), and the supernatant was collected. Cell extracts (30 µg of protein) were analyzed by sodium dodecyl sulfate–polyacrylamide gel electrophoresis on 4–12% gradient gels (Invitrogen NuPAGE system) and the resulting bands were transferred onto nitrocellulose membranes (0.45 µM). The membranes were blocked by incubation for 1 h at room temperature with Tris-buffered saline supplemented with 0.1% Tween 20 (TBS-T: 20 mM Tris–HCl, pH 7.5, 100 mM NaCl, 0.1% Tween 20) and 5% bovine serum albumin, and then incubated overnight with primary antibodies (1/1000) in TBS-T supplemented with 5% bovine serum albumin, at 4°C. The membranes were then washed in TBS-T and incubated with horseradish peroxidase (HRP)-conjugated secondary antibodies for 1 h at room temperature. Signals were detected with the ECL detection system, following the exposure of Fujifilm LAS-300, Fujifilm Medical Systems, Stamford, CT, USA. We used β-actin detection to check for equal protein loading and transfer efficiency. The densitometry data obtained were analyzed with ImageJ software and normalized relative to the density of β-actin.

2.5. Absolute quantification of mRNA copy number

Specific 250 to 1000 bp amplicons were generated from the RNA by RT-PCR and purified. Each amplicon was assayed and the number of copy was calculated according to its size in bp. Serial dilutions of known concentration were used in qPCR, to determine the fit

coefficients of the relative standard curve. Absolute quantification was performed by interpolation of the PCR signal (Cq) into this standard curve with the Livak-Schmittgen equation [**23**]. The forward and reverse primers used were as follows: PKACα, cccgttcctggtcaaacttg, ggggtgtggagtggatgtta; PKACβ cgaagtggagagcgtgaaag, gtcttgatgtcactcacgcc; PKAR1α, gcgctgaggtttacactgag, tctcagacggacagtgacac; PKAR1β, cacactgaggaaacgcaaga, catagggaatgggtcacagg; PKAR2α, caataccccgagagctgcta, gaagcaaagtggaaggtggg; PRKAR2β, ggtcaaagaaggggaacacg, taactgcttcactaacgcgc.

2.6. Quantitative PCR assay

Total RNA was extracted with the Reliaprep™ RNA isolation kit from Promega, Charbonnieres, France. Total RNA (0.5-1 µg) was reverse-transcribed with the M-MLV reverse transcriptase system and 1 µM Oligo-dT (Invitrogen, Saint Aubin, France). We carried out qPCR with primers designed with the Roche Universal Probe Library Assay Design Center, with a LightCycler® 480SYBR Green I Master system (Roche Diagnostics, Meylan, France). Cyclophilin A (CycloA) was used as the housekeeping gene. PCR was performed with the following thermal settings: denaturation and enzyme activation at 95°C for 5 min, followed by variable numbers of cycles of 95°C for 10 s, 60°C for 15 s, and 72°C for 10 s. Amplification was monitored online and the reaction was stopped at the end of the logarithmic phase. Melting curve analysis was carried out to check the specificity of PCR. Controls and water blanks were included in each run, and all gave negative results. The qPCR analysis of serial dilutions of a mixture of cDNAs indicated that amplification efficiency was close to 100% for all the genes studied. The primer sequences used to amplify the cDNAs are shown in **Table 1**.

2.7. Cytokine array

Conditioned medium from cultures of VSMCs treated with vehicle, IL-1β (5 ng/ml), TNFα (10 ng/ml) or IFNγ (10 ng/ml) for 72h was incubated with Proteome Profiler Rat Cytokine Array Panel A membranes (R&D Systems, Minneapolis, Minnesota, USA). These concentrations of cytokines were used throughout the study.

2.8. Immunocytochemistry

Collagen-coated coverslips were seeded with 5000 cells/cm^2. The cells were grown to confluence and starved of serum, and they were then treated for 72 h with recombinant IL-1β, TNFα or IFNγ. Cells were fixed by incubation in 2% sucrose and 3% paraformaldehyde in PBS for 15 min at room temperature, and permeabilized by incubation with 0.2% Triton X-100 in PBS for 5 min. Non-specific sites were blocked by incubation with 5% FCS in PBS.

The cells were stained for actin and vinculin, by incubation for 2 h at 21°C with Alexa Fluor® 594-conjugated phalloidin and an FITC-conjugated monoclonal anti-vinculin antibody, in PBS containing 5% FCS. The cell nuclei were stained with 4',6'-diamidino-2-phenylindole (DAPI). The coverslips were mounted in Dako fluorescence mounting medium (Dako, Carpinteria, California, USA) and examined with a Nikon Diaphot 300 microscope (Nikon, Tokyo, Japan).

2.9. PGE_2 assay

PGE_2 secretion was evaluated with an enzyme immunoassay kit from Cayman Chemical SPI-BIO, Massy, France.

2.10. Generation of $^{T}Epac^{VV}$ cAMP biosensor-encoding adenovirus

$^{T}Epac^{VV}$, a FRET-based sensor for cAMP, consists of a cAMP-binding domain from the exchange protein directly activated by cAMP 1 (Epac1) sandwiched between the fluorescent donor (mTurquoise (cyan) and acceptor cpVenus-Venus (yellow) proteins [**24**]. The cDNA encoding the $^{T}Epac^{VV}$ biosensor was inserted between the *Bgl*II and *Xho*I restriction sites of the pShuttle plasmid (Agilent Biotechnology, Santa Clara, California, USA). The pShuttle- $^{T}Epac^{VV}$ was linearized by digestion with *Pme*I and inserted into the pAdEasy-1 vector by homologous recombination. Recombinant viral vectors carrying the $^{T}Epac^{VV}$ biosensor were produced in the HEK-293T cell line at UMR1089, Nantes, France.

2.11. Dynamics of cAMP production

VSMCs on collagen-coated glass coverslips were incubated with the $^{T}Epac^{VV}$-encoding adenoviral vector (~100 particles per cell) for 24 h at 37°C, under an atmosphere containing 5% CO_2. Coverslips were placed in a microscope chamber, continuously perfused (2 ml/min) with a buffer containing 125 mM NaCl, 2 mM $CaCl_2$, 1 mM $MgCl_2$, 1.25 mM NaH_2PO_4, 26 mM $NaHCO_3$, 25 mM glucose and maintained at 32°C, saturated with 5% CO_2–95% O_2. TNFα, IFNγ or IL-1β was added during the perfusion.

Conditioned medium for the FRET experiments was obtained by treating VSMCs with IL-1β, TNFα or IFNγ for 72 h in FluoroBrite™ DMEM, a medium specially developed for the fluorescence imaging of live cells. We analyzed the dynamics of cAMP production after the addition of conditioned medium, in cells that had previously undergone transdifferentiation in response to exposure to IL-1β, TNFα or IFNγ for 48h and had then been starved overnight. Ratiometric analyses were performed as follows: fluorescence was induced at an excitation wavelength of 435 nm, and the fluorescence emitted by the donor and acceptor was monitored with a dichroic mirror (455 DCLP) and alternating emission filters for CFP (470±20 nm) and YFP (530±25 nm). Pairs of images were recorded with a CCD

camera (Orca-ER, Hammamatus), at 20-second intervals. Changes in intracellular [cAMP] are expressed as the ratio of CFP fluorescence (F480nm) to YFP fluorescence (F535nm). The ratios were multiplied by a constant such that the baseline ratio was 1 in basal conditions. The maximum ratio change (Rmax) was obtained by stimulating cells with 10 μM FSK and 200 μM IBMX. The data shown are representative of three independent experiments, with the acquisition of 10-15 cells per experiment.

2.10. Time-lapse video microscopy

Sixteen hours before any treatment, cells were starved in serum-free DMEM. Changes in their morphology were then monitored by time-lapse video microscopy. Phase-contrast images (3 fields/well) were captured with a 20x objective, at 2.5-minute intervals, for 18 h. Images were captured with an inverted microscope (DMI 6000B from Leica) equipped with a cell incubation chamber, a motorized stage, and a coolSNAP HQ2 CCD camera. All operations were controlled with Metamorph software (version 7.1).

2.11. Statistics

All data are presented as means ± SEM of at least three independent experiments. Graphical representations were generated and the statistical significance of differences between groups were assessed with GraphPad Prism 5 (GraphPad Software, Inc., La Jolla, CA, USA). Pairwise comparisons of groups were carried out with two-tailed Mann-Whitney tests. For comparisons of multiple groups, we used Kruskal-Wallis tests followed by Dunn's multiple comparison tests. Differences were considered significant if $P < 0.05$.

3. Results

3.1. IL-1β increases intracellular [cAMP] *via* one or several autocrine/paracrine factors

Light microscopy (**Figure 1A and Supplementary Videos 1-4)** showed that IL-1β was the only cytokine of those tested capable of inducing the transition to a stellate form in VSMCs. *In vitro*, this phenomenon peaks about 12 hours after stimulation, tending to decrease thereafter, as shown by time-lapse imaging. It is followed by a second wave of transition to a stellate morphology beginning 48 h after the addition of IL-1β and intensifying until 72 h after the addition of this cytokine. The cAMP-dependent stellate morphology of VSMCs (induced by the β-adrenergic receptor agonist isoproterenol) is characterized by a loss of focal adhesions and the disassembly of actin stress fibers [**20**]. We therefore also stained cells for actin and the focal adhesion marker vinculin. IL-1β disrupts focal adhesions and actin stress fibers, whereas neither TNFα nor IFNγ modifies the cytoskeleton (**Figure 1B).** However, the treatment of VSMCs with IL-1β, TNFα or IFNγ for 48 h, followed by an analysis of mRNA levels for four major contractile markers showed that all these cytokines inhibited the expression of at least some of these markers, attesting to their efficacy. All three compounds decreased the levels of SM-MHC and calponin (**Supplementary Figure S2**), but only IL-β and TNFα decreased SM22 (by ~90 and 50%, respectively) and smoothelin (by ~75 and 50%, respectively) mRNA levels to any great extent. Consistent with a cAMP-dependent phenomenon, stellate cells were also obtained following an increase in intracellular [cAMP] induced by forskolin (FSK), a specific activator of adenylyl cyclases (ACs). This effect was observed within a few minutes of FSK application and was maintained for up to 4 h (**Supplementary Figure 1B and Supplementary Video 5**). Together with the demonstration that IL-1β was the only cytokine of those tested to increase PKA activity significantly (as shown by measuring the phosphorylation of PKA substrates, **Figure 2**), these data demonstrate that IL-1β-induced VSMC transdifferentiation is different from that induced by the other cytokines tested. These data also suggest that this effect is at least partly dependent on the cAMP signaling pathway.

We investigated whether the IL-1β-dependent transdifferentiation of VSMCs was associated with an increase in intracellular cAMP concentration, using the FRET biosensor $^{T}Epac^{VV}$ [**21**]. We monitored changes in intracellular cAMP concentration by calculating the ratio of CFP fluorescence (F480nm) to YFP (F535nm) fluorescence. The baseline ratio at the start of the experiment was set to 1 and the maximum ratio change (Rmax) was systematically determined at the end of the experiment, by adding 10 µM forskolin and 200 µM isobutyl-L-

methylxanthine (IBMX), a broad-spectrum phosphodiesterase inhibitor. Incubation with isoproterenol (used as a positive control) greatly increased the ratio to 90.0 ± 1.1% of the maximal ratio change (n=4, P < 0.001),,but none of the cytokines tested induced a detectable increase in intracellular [cAMP] over a similar timeframe (**Figure 3**). Given the time taken for IL-1β to induce the transition to a stellate cell morphology, we hypothesized that any increase in cAMP concentration might be dependent on the production of autocrine/paracrine factors. We used conditioned medium obtained from VSMCs treated with vehicle, IL-1β, TNFα or IFNγ for 72 h (referred to as vehicle-CM, IL-1β-CM, TNFα-CM and IFNγ-CM, respectively) to test this hypothesis. IL-1β-CM immediately triggered a large increase in intracellular cAMP concentration (up to 34.5 ± 3.8% of the maximum ratio, n = 4, P < 0.01), whereas the other conditioned media had no effect on cAMP (**Figure 4 (left and middle panels) and Table 2)**. Consistent with this finding, the addition of IL-1β-CM added to naive/contractile cells also rapidly (within less than 2 hours) triggered the transition to a stellate cell morphology (**Figure 4B, right panels**), whereas treatment with IL-1β took at least 12 hours to achieve the same effect (**Figure 1A**). The other two conditioned media (TNFα-CM and IFNγ-CM) were inefficient regardless of the mode of monitoring used (dynamics of cAMP production or change in cell shape)**.** Thus, stimulation with IL-1β leads to the release of one or several autocrine/paracrine factors, triggering an increase in the intracellular concentration of cAMP. These findings also demonstrate that cAMP production is a hallmark of IL-1β-dependent VSMC transdifferentiation.

3.2. The IL-1β-dependent increase in intracellular [cAMP] involves PGE_2 secretion and PGE_2 receptor isoform 4 (EP4)

As a first step towards identifying the factors involved, we compared the secretion profiles of IL-1β, TNFα and IFNγ, in terms of their induction of the inflammatory cytokines/chemokines and enzymes involved in eicosanoid/PGE_2 synthesis at the mRNA and/or protein level. For most of the mRNAs studied, significant induction was observed with at least two of the cytokines tested, IL-1β and TNFα, or IFNγ and TNFα, indicating a very low likelihood of a role in stellate cell morphology for these mRNAs (**Table 3** and **Figure 5 left panels A and B)**. However, the mRNAs encoding COX-2, CCL3, and VEGF-A were specifically and significantly induced by IL-1β. It was also clear from our results that i) TNFα was the most potent cytokine for CCL5 mRNA synthesis; ii) IFNγ, which had no effect on the CCL5, CCL3, COX-2 and VEGF-A mRNAs, strongly induced synthesis of the CXCL10 mRNA encoding the chemo-attractant of T lymphocytes and monocytes. Using a

cytokine array allowing the detection of 29 different inflammatory mediators and a PGE_2 assay, we were able to expand our results further, to show that, in addition to triggering the expression of CCL3 and VEGF, IL-1β also induced high levels of CXCL2, GM-CSF and IL6 expression, and PGE_2 secretion. It is also clear that i) IFNγ induces the production of small amounts of CXCL1, CX3CL1 and CCL5; ii) contractile vehicle-treated VSMCs have very low levels of secretory activity, because only CXCL1 and the tissue inhibitor matrix metalloproteinase-1 are detected in their culture medium.

Our data and those obtained for human VSMCs [**25**] suggested that PGE_2 was a potentially good candidate for relaying the increase in cAMP concentration in response to IL-1β, particularly as PGE_2 triggered the transition to a stellate VSMC morphology within an hour, or even faster in some cases, depending on the number of cell subcultures (**Supplementary Video 6**). We therefore repeated the experiments carried out with IL-1β-CM, successively blocking each of the three PGE_2 receptors expressed by VSMCs[1]. Each dose of antagonist was selected on the basis of published data, to yield maximal inhibition corresponding to 20 times the Ki value [**26-28**]. Neither the EP1 antagonist nor the EP3 antagonist (SC51322, L798,106, respectively) affected the increase in intracellular [cAMP] induced by IL-1β-CM (**Figure 6A and C).** Conversely, when the EP4 antagonist ONO AE3208 was applied, intracellular [cAMP] rapidly (within 2 minutes) returned to baseline levels. Consistently with the observation that the transition to a stellate shape was associated with an increase in intracellular [cAMP], ONO AE3 was the only compound capable of blocking this process efficiently in IL-1β-CM- or PGE_2-treated cells. In light of these findings and the observation that very similar results were obtained when IL-1β-CM was replaced with PGE_2 (**Figure 6B and D**), we conclude that the autocrine/paracrine factor secreted upon IL-1β stimulation in VSMCs is unique and can be identified as PGE_2.

3.3. The transition to a stellate morphology in VSMCs involves PKA

The regulation of cellular properties by cAMP is mediated principally by cyclic nucleotide-gated ion channels, the exchange proteins directly activated by cAMP (Epac-1 and -2)[2] and/or protein kinase A (PKA). The treatment of naïve/contractile VSMCs with

[1]Type E_2 prostaglandin may activate neighboring cells through four different G protein-coupled receptor subtypes, EP1-4. Each of these receptor subtypes is encoded by a different gene and has unique pharmacological features. Contractile and fully secretory rat VSMCs (obtained by incubation with 10 ng/ml IL-1β, 72 h) express the same pattern of PGE_2 receptor subtype transcript production: 1, 3, 4, but not 2 (**Purdy and Arendshorst, 2000; Clément *et al.*, 2006**).

[2]Epacs are GDP/GTP exchange factors for small G proteins of the Ras family, including Rap1A and B, Rap2A and B, and Hras (*Schmidt, M., F.J. Dekker, and H. Maarsingh, Exchange protein directly activated by cAMP*

increasing doses of 6BNZ (a specific activator of PKA) led to a dose-dependent increase in the number of stellate cells (**Figure 7A**); 8-pCPT-O-Me-cAMP, an activator of Epac, was ineffective up to a dose of 500 μM. The specificity of 6BNZ was confirmed by the prevention of its effects on cell morphology at a concentration of 250 μM by the prior treatment of cells with various doses (100-500 μM) of Rp-8-Br-cAMP (**Supplementary Figure S3**) or RP-8-CP-cAMP (**data not shown**), both of which inhibit PKA. The treatment of VSMCs allowed to transdifferentiate in the presence of IL-1β (5 ng/ml for 48 h) with 100 μM 6BNZ for 3 h greatly increased the number of stellate cells (**Figure 7B**). By contrast, the same concentration of 6BNZ had almost no effect on contractile/naive cells (**Figure 7A**). Epac stimulation of VSMCs transdifferentiating in response to IL-1β had no effect, regardless of the batch of 8-pCPT-O-Me-cAMP used (**Figure 7B**). These results suggest that the IL-1β-induced/cAMP-dependent change in shape of VSMCs is mediated by PKA activation.

PKA is a holoenzyme with four subunits, two of which are catalytic, the other two being regulatory. The association of regulatory subunits R1α/R1β with any of the catalytic subunits (Cα, Cβ or Cγ) defines PKA1, whereas an association of the regulatory subunits R2α/R2β with any of the catalytic subunits results in PKA2 and an inhibition of catalytic activity [**29**]. These two enzymes also differ in terms of their location and affinity for cAMP. Rodents lack the catalytic subunit Cγ. A comparison of mRNA levels for each of the subunits between naive/contractile and IL-1β-treated VSMCs showed that the contractile/naïve VSMCs produced all four regulatory (R) subunits, the most abundant being R1α (~65%), followed by R2α (~22%), R2β (~10%) and R1β (~3 %); Cα and Cβ accounted for ~70% and 30% of catalytic subunits, respectively (**Figure 7C, left panel**). IL-1β treatment induces a significant 40-fold increase in R1β gene expression 48 h after stimulation (**Figure 7C, left panel**), but R1α expression nevertheless predominated. The levels of R2α and R2β mRNA were affected much less, if at all, by IL-1β. An analysis of catalytic subunit expression during the process of transdifferentiation revealed no change in the pattern of expression, regardless of the cytokine used (**Figure 7C left panel** and **data not shown)**. Based on these data, we decided to silence R1α to confirm the involvement of PKA in this process. In many cell types and *in vivo*, the disruption of PKAR1α is associated with an increase in the catalytic activity of PKA [**30-32**]. Consistent with a role for PKA in stellate cell morphology, knocking down R1α expression

(epac): a multidomain cAMP mediator in the regulation of diverse biological functions. Pharmacol Rev, 2013. 65(2): p. 670-709).

mimicked the effect of IL-1β/PGE_2 on cell morphology, resulting in destabilization of the actin cytoskeleton and focal adhesions (as shown by immunostaining for F-actin and vinculin, respectively). Conversely, knocking down R1β expression had no impact (**Figure 7D and Supplementary Figure S4B)**. Despite the increase in R1β mRNA levels observed on IL-1β treatment, the silencing of R1β in PGE_2-treated cells did not prevent these cells from developing a stellate phenotype. The efficacy and specificity of R1α and β siRNAs were demonstrated by the determination of R1α and β mRNA levels after transfection (**Supplementary Figure S4A**).

4. Discussion

The transdifferentiation of VSMCs in the inflammatory context of atherogenesis plays a key role in atherosclerosis, as highlighted by the recent study by Shankman *et al.,* 2015 [**15**]. Indeed, these authors showed that the contribution of VSMCs to atherosclerotic lesions had been greatly underestimated, due to their ability to develop the expression of macrophage, mesenchymal stem cell and/or myofibroblast markers in lesions. Given the known role of pancreatic stellate cells in acute episode of pancreatic injury [**33**], it is possible that the stellate cells of the artery wall serve as extracellular matrix-producing cells or myofibroblasts, increasing plaque stability. However, chronic IL-1β-treatment reduces the expression by VSMCs of profibrotic and/or proproliferative compounds, such as connective tissue growth factor and insulin growth factor-1 (**Blirando *et al.* unpublished data**). It therefore appears more likely that the aortic stellate cells first produce large amounts of ECM proteins and then undergo a switch towards a phenotype with high levels of MMP activity. This remains to be demonstrated, but is consistent with the two waves of stellate cell development observed *in vitro* in response to short- and long-term stimulation with IL-1β.

We show that, of the three key pro-atherogenic cytokines tested (IL-1β, TNFα and IFNγ), IL-1β was the most potent inducer (in terms of the numbers and amounts of secreted molecules) of the VSMC inflammatory response, triggering the release of substantial amounts of CCL3, GM-CSF, IL-6, VEGF-α, CX3CL1, CXCL1, CXCL5 and PGE_2. Consistent with published findings, IFNγ was the most efficient of the molecules tested for inducing CXCL10 expression in VSMCs [**34**] and TNFα was a stronger inducer of CCL5 mRNA production than IL-1β [**35**]. Our findings also demonstrate that IL-1β was the only one of the molecules tested able to trigger the disruption of focal adhesions and actin stress fibers, leading to a cAMP-dependent transition to a stellate morphology, as observed in atherosclerotic lesions [**14, 20**]. Finally, using the FRET-based cAMP biosensor $^{T}Epac^{vv}$ and a battery of pharmacological compounds, we were able to link this cAMP-dependent phenomenon to the autocrine/paracrine factor PGE_2, which is released upon IL-1β stimulation and the activation of PKA by the EP4 prostaglandin receptor

The IL-1β-induced increase in intracellular [cAMP] mediated by the release of the autocrine/paracrine factor PGE_2 is consistent with i) the time lag (12 h) observed between the start of IL-1β-treatment and the development of a cAMP-dependent stellate cell morphology; ii) our previous results showing that PGE_2 acts in synergy with IL-1β to enhance the

phenotypic transition in smooth muscle cells [**22**]. It is also consistent with published data showing that the IL-1β-mediated increase in cAMP concentration in VSMCs is due to the ability of IL-1β to trigger prostaglandin release [**25, 36**].

Consistent with many other studies showing that EP4 activation leads to an increase in intracellular [cAMP] [**37**], we showed, by successively blocking each of the EP receptors expressed in VSMCs, that the Gs-coupled EP receptor subtype 4 was involved in the increase in cAMP concentration and the transition to a stellate cell morphology. Following the addition of PGE_2 in conditions of EP receptor subtype 3 blockade, we observed a slight (but non-significant) decrease in cAMP production (**Figure 6B**), leading the generation of fewer stellate VSMCs (**Figure 6F**, panels PGE2 *vs.* PGE2 +L-798, 106). This finding is consistent with our previous report showing that, in IL-1β-treated cells, the PGE_2-dependent increase in cAMP concentration results from activation of the EP4 and EP3 receptors [**22**]. Indeed, transdifferentiation is associated with a change in the regulation (negative to positive) of the G_i-coupled receptor EP3, potentiating the cAMP produced by G_s-coupled EP4 receptors. One reasons for the lack of significant results for the EP3 antagonist is that monitoring the dynamics of cAMP production by FRET requires the removal of IL-1β from the culture medium 24 h before the experiment. The VSMCs transdifferentiating in response to IL-1β may, therefore display partial reversion towards a quiescent phenotype, accounting for the small contribution of EP3 to the PGE_2-induced increase in cAMP levels and changes in morphology.

Using the 6BNZ-cAMP (a PKA activator), a siRNA directed against the most abundant PKA regulatory subunit, R1α, and 8-pCPT-O-Me-cAMP (an Epac activator), we demonstrated the specific involvement of PKA in the cAMP-dependent transition towards a stellate cell phenomenon. However according to Hewer *et al*., (2011), this transition towards a stellate phenotype in VSMCs results from a synergic activation of PKA and Epac not involving the Epac-dependent Rap1 protein [**38**]. Several studies have reported Rap1-independent effects of Epac [**39, 40**], but Epac activation generally leads to a Rap1-mediated GDP/GTP exchange [**41**]. Furthermore, Hewer *et al.*, reported, for 8-pCPT-O-Me-cAMP, a trend towards increasing levels of focal adhesion, a result conflicting with the effects of 8-pCPT-O-Me-cAMP on stellate cell morphology that they report. Thus, for the conclusive implication or exclusion of a role for Epac in this process, further evaluations are required of the possible activation of other downstream Epac effectors, such as the Rit small GTPase or the c-June N-terminal kinase, in response to PGE_2 treatment.

As mentioned above, the disruption of PKAR1α *in vivo* is associated with an increase in the catalytic activity of PKA [**30-32**], and this increase in catalytic activity (which is lethal in the embryo due to the failure to establish mesoderm-derived structures) is partially rescued by eliminating the PKA catalytic subunit α [**42**], providing evidence for a causal relationship between the elimination of PKAR1α and the increase in PKA catalytic activity. Embryonic fibroblasts from PKAR1α$^{-/-}$ mouse embryos display similar changes in morphology to VSMCs in which R1α is silenced, with a decrease in activated Rac levels [**32**]. Moreover, the transition of VSMCs to a stellate morphology induced by agents increasing cAMP levels, such as isoproterenol and forskolin, can be prevented by the expression of an activated form of Rac1. Conversely, the pharmacological inhibition of Rac1 or the expression of a dominant negative form of Rac1 is sufficient to induce the transition to a stellate phenotype [**20**]. Finally, PKAR1α disruption in Schwann cells is associated with a decrease in the formation of lamellopodia [**31**], a process involving Rac1 activation [**43**]. This suggests a role for Rac1 in the PGE_2/cAMP-dependent development of stellate morphology in VSMCs. Furthermore, as PKA phosphorylates key actors involved in cytoskeletal regulation, such as the vasodilator-stimulated phosphoprotein (VASP) [**18**], Ras homolog gene family member A (RhoA) [**44**] and LIM domain kinase 1 (LIMK1) [**32**], these proteins may also be involved in the cAMP-dependent transition to a stellate phenotype. In any event, PKA enhances this process by phosphorylating globular actin (G-actin), thereby decreasing filamentous actin (F-actin) formation [**44**]. Indeed, PKAR1α silencing induced a destabilization of filamentous actin and the disassembly of focal adhesions (**Figure 7C**).

IL-1β-dependent transdifferentiation is associated with an increase in PKAR1β gene expression. Nevertheless, the silencing of this subunit does not prevent VSMCs from undergoing the transition to a stellate phenotype following stimulation with PGE_2 (**Figure 7B**). We therefore conclude that PKAR1β is not required for this process.

PKA containing PKAR1β subunits has been shown to be activated at cAMP concentrations lower, by a factor of three to seven, than those activating PKAR1α [**45**]. Therefore PKA-dependent responses should be even more sensitive to any increase in intracellular cAMP concentration in VSMCs undergoing transdifferentiation in response to IL-1β. Interestingly, in PKAR1β-knockout mice, inflammation and nociceptive pain levels are low in a model of paw edema and pain behavior induced by formalin injection [**46**]. In addition, patients with systemic lupus erythematosus present a downregulation of PKAR1β expression and lower levels of IL-2 secretion by T lymphocytes, these deficits possibly being rescued by PKAR1β

gene transfer [**47**]. The data presented here are consistent with a role for PKAR1β in the increase in cAMP concentration mediating VSMC inflammation and, possibly, PGE_2 secretion.

5. Conclusions and future prospects

VSMC transdifferentiation in response to exposure to pro-atherogenic stimuli, such as the cytokines IL-1β, TNFα and IFNγ, is a key event in the initiation and further development of atherosclerosis. We demonstrate here that IL-1β contributes to this transdifferentiation process not only by decreasing the expression of contractile markers, but also by disrupting F-actin and focal adhesions through the release of PGE_2 and subsequent cAMP pathway activation. Given these and published findings, it will be of interest to investigate the effect on plaque development of VSMC-directed PKAR1α and/or PKAR1β gene knockout in atherosclerosis-susceptible mouse models. Indeed, such studies should define the roles of these molecules in the onset of atherosclerosis and their potential relevance as treatment targets. Studies on human atherothrombotic plaques should provide insight into the relationship between PKAR1α and/or PKAR1β expression and vulnerability to plaque formation. They should also provide a more general view of the role of this relationship in human atherosclerosis.

Acknowledgments

We thank Susanne Bolte, Richard Schwartzmann and Jean-François Gilles from the imaging facility of the Paris-Seine Biological Institute (IBPS). This work was supported by Paris VI University and the national research agency, under grant number 11 BSV1 034 01.

References

[1] P. Libby, P. M. Ridker and G. K. Hansson, Progress and challenges in translating the biology of atherosclerosis., Nature 473 (2011) 317-325.

[2] K. Sakakura, M. Nakano, F. Otsuka, E. Ladich, F. D. Kolodgie and R. Virmani, Pathophysiology of atherosclerosis plaque progression., Heart Lung Circ 22 (2013) 399-411.

[3] B. Legein, L. Temmerman, E. A. Biessen and E. Lutgens, Inflammation and immune system interactions in atherosclerosis., Cell Mol Life Sci 70 (2013) 3847-3869.

[4] G. K. Hansson and A. Hermansson, The immune system in atherosclerosis., Nat Immunol 12 (2011) 204-212.

[5] J. E. McLaren and D. P. Ramji, Interferon gamma: a master regulator of atherosclerosis., Cytokine Growth Factor Rev 20 (2009) 125-135.

[6] P. Hellstrand and S. Albinsson, Stretch-dependent growth and differentiation in vascular smooth muscle: role of the actin cytoskeleton., Can J Physiol Pharmacol 83 (2005) 869-875.

[7] C. P. Mack and J. S. Hinson, Regulation of smooth muscle differentiation by the myocardin family of serum response factor co-factors., J Thromb Haemost 3 (2005) 1976-1984.

[8] M. S. Parmacek, Myocardin-related transcription factors: critical coactivators regulating cardiovascular development and adaptation., Circ Res 100 (2007) 633-644.

[9] J. Shen, M. Yang, D. Ju, H. Jiang, J. P. Zheng, Z. Xu and L. Li, Disruption of SM22 promotes inflammation after artery injury via nuclear factor kappaB activation., Circ Res 106 (2010) 1351-1362.

[10] J. Shen, M. Yang, H. Jiang, D. Ju, J. P. Zheng, Z. Xu, T. D. Liao and L. Li, Arterial injury promotes medial chondrogenesis in Sm22 knockout mice., Cardiovasc Res 90 (2011) 28-37.

[11] M. F. Carlier, J. Pernier, P. Montaville, S. Shekhar and S. Kuhn, Control of polarized assembly of actin filaments in cell motility., Cell Mol Life Sci (2015)

[12] S. J. Gunst and W. Zhang, Actin cytoskeletal dynamics in smooth muscle: a new paradigm for the regulation of smooth muscle contraction., Am J Physiol Cell Physiol 295 (2008) C576-C587.

[13] M. A. Schwartz and R. K. Assoian, Integrins and cell proliferation: regulation of cyclin-dependent kinases via cytoplasmic signaling pathways., J Cell Sci 114 (2001) 2553-2560.

[14] A. N. Orekhov, E. R. Andreeva, A. V. Krushinsky, I. D. Novikov, V. V. Tertov, G. V. Nestaiko, K. Khashimov, V. S. Repin and V. N. Smirnov, Intimal cells and atherosclerosis. Relationship between the number of intimal cells and major manifestations of atherosclerosis in the human aorta., Am J Pathol 125 (1986) 402-415.

[15] L. S. Shankman, D. Gomez, O. A. Cherepanova, M. Salmon, G. F. Alencar, R. M. Haskins, P. Swiatlowska, A. A. Newman, E. S. Greene, A. C. Straub, B. Isakson, G. J. Randolph and G. K. Owens, KLF4-dependent phenotypic modulation of smooth muscle cells has a key role in atherosclerotic plaque pathogenesis., Nat Med 21 (2015) 628-637.

[16] E. Seki and D. A. Brenner, Recent advancement of molecular mechanisms of liver fibrosis., J Hepatobiliary Pancreat Sci 22 (2015) 512-518.

[17] G. N. Chaldakov, T. Nabika, Y. Nara and Y. Yamori, Cyclic AMP- and cytochalasin B-induced arborization in cultured aortic smooth muscle cells: its cytopharmacological characterization., Cell Tissue Res 255 (1989) 435-442.

[18] R. Gros, Q. Ding, J. Chorazyczewski, J. G. Pickering, L. E. Limbird and R. D. Feldman,

Adenylyl cyclase isoform-selective regulation of vascular smooth muscle proliferation and cytoskeletal reorganization., Circ Res 99 (2006) 845-852.
[19] T. Nabika, P. A. Velletri, T. Igawa, Y. Yamori and W. Lovenberg, Comparison of cyclic AMP accumulation and morphological changes induced by beta-adrenergic stimulation of cultured vascular smooth muscle cells and fibroblasts., Blood Vessels 22 (1985) 47-56.
[20] S. Pelletier, C. Julien, M. R. Popoff, N. Lamarche-Vane and S. Meloche, Cyclic AMP induces morphological changes of vascular smooth muscle cells by inhibiting a Rac-dependent signaling pathway., J Cell Physiol 204 (2005) 412-422.
[21] J. Klarenbeek and K. Jalink, Detecting cAMP with an EPAC-based FRET sensor in single living cells., Methods Mol Biol 1071 (2014) 49-58.
[22] N. Clement, M. Glorian, M. Raymondjean, M. Andreani and I. Limon, PGE2 amplifies the effects of IL-1beta on vascular smooth muscle cell de-differentiation: a consequence of the versatility of PGE2 receptors 3 due to the emerging expression of adenylyl cyclase 8, J Cell Physiol 208 (2006) 495-505.
[23] K. J. Livak and T. D. Schmittgen, Analysis of relative gene expression data using real-time quantitative PCR and the 2(-Delta Delta C(T)) Method., Methods 25 (2001) 402-408.
[24] J. B. Klarenbeek, J. Goedhart, M. A. Hink, T. W. Gadella and K. Jalink, A mTurquoise-based cAMP sensor for both FLIM and ratiometric read-out has improved dynamic range., PLoS One 6 (2011) e19170.
[25] D. Beasley, COX-2 and cytosolic PLA2 mediate IL-1beta-induced cAMP production in human vascular smooth muscle cells., Am J Physiol 276 (1999) H1369-H1378.
[26] E. A. Hallinan, A. Stapelfeld, M. A. Savage and M. Reichman, 8-chlorodibenz[b,f][1,4]oxazepine-10(11H)-carboxylic acid,2-[3-[2-(furanylmethyl)thio]-1 oxopropyl]hydrazide (SC-51322): A potent PGE2 antagonist and analgesic, Bioorganic & Medicinal Chemistry Letters 4 (1994) 509-514.
[27] H. Juteau, Y. Gareau, M. Labelle, C. F. Sturino, N. Sawyer, N. Tremblay, S. Lamontagne, M. C. Carriere, D. Denis and K. M. Metters, Structure-activity relationship of cinnamic acylsulfonamide analogues on the human EP3 prostanoid receptor., Bioorg Med Chem 9 (2001) 1977-1984.
[28] K. Kabashima, T. Saji, T. Murata, M. Nagamachi, T. Matsuoka, E. Segi, K. Tsuboi, Y. Sugimoto, T. Kobayashi, Y. Miyachi, A. Ichikawa and S. Narumiya, The prostaglandin receptor EP4 suppresses colitis, mucosal damage and CD4 cell activation in the gut., J Clin Invest 109 (2002) 883-893.
[29] S. S. Taylor, R. Ilouz, P. Zhang and A. P. Kornev, Assembly of allosteric macromolecular switches: lessons from PKA., Nat Rev Mol Cell Biol 13 (2012) 646-658.
[30] X. Cheng, Z. Ji, T. Tsalkova and F. Mei, Epac and PKA: a tale of two intracellular cAMP receptors., Acta Biochim Biophys Sin (Shanghai) 40 (2008) 651-662.
[31] L. Guo, A. A. Lee, T. A. Rizvi, N. Ratner and L. S. Kirschner, The protein kinase A regulatory subunit R1A (Prkar1a) plays critical roles in peripheral nerve development., J Neurosci 33 (2013) 17967-17975.
[32] K. S. Nadella, M. Saji, N. K. Jacob, E. Pavel, M. D. Ringel and L. S. Kirschner, Regulation of actin function by protein kinase A-mediated phosphorylation of Limk1., EMBO Rep 10 (2009) 599-605.
[33] J. S. Wilson, R. C. Pirola and M. V. Apte, Stars and stripes in pancreatic cancer: role of stellate cells and stroma in cancer progression., Front Physiol 5 (2014) 52.
[34] X. Wang, T. L. Yue, E. H. Ohlstein, C. P. Sung and G. Z. Feuerstein, Interferon-inducible protein-10 involves vascular smooth muscle cell migration, proliferation, and

inflammatory response., J Biol Chem 271 (1996) 24286-24293.
[35] N. J. Jordan, M. L. Watson, R. J. Williams, A. G. Roach, T. Yoshimura and J. Westwick, Chemokine production by human vascular smooth muscle cells: modulation by IL-13., Br J Pharmacol 122 (1997) 749-757.
[36] D. Beasley and M. E. McGuiggin, Interleukin 1 induces prostacyclin-dependent increases in cyclic AMP production and does not affect cyclic GMP production in human vascular smooth muscle cells., Cytokine 7 (1995) 417-426.
[37] S. Narumiya, Y. Sugimoto and F. Ushikubi, Prostanoid receptors: structures, properties, and functions., Physiol Rev 79 (1999) 1193-1226.
[38] R. C. Hewer, G. B. Sala-Newby, Y. J. Wu, A. C. Newby and M. Bond, PKA and Epac synergistically inhibit smooth muscle cell proliferation., J Mol Cell Cardiol 50 (2011) 87-98.
[39] D. Hochbaum, T. Tanos, F. Ribeiro-Neto, D. Altschuler and O. A. Coso, Activation of JNK by Epac is independent of its activity as a Rap guanine nucleotide exchanger., J Biol Chem 278 (2003) 33738-33746.
[40] G. X. Shi, H. Rehmann and D. A. Andres, A novel cyclic AMP-dependent Epac-Rit signaling pathway contributes to PACAP38-mediated neuronal differentiation., Mol Cell Biol 26 (2006) 9136-9147.
[41] S. S. Roscioni, C. R. Elzinga and M. Schmidt, Epac: effectors and biological functions., Naunyn Schmiedebergs Arch Pharmacol 377 (2008) 345-357.
[42] L. S. Kirschner, Z. Yin, G. N. Jones and E. Mahoney, Mouse models of altered protein kinase A signaling., Endocr Relat Cancer 16 (2009) 773-793.
[43] A. N. Lyle and W. R. Taylor, RACing up a new regulatory mechanism for vascular smooth muscle cell migration., Arterioscler Thromb Vasc Biol 33 (2013) 667-669.
[44] A. K. Howe, Regulation of actin-based cell migration by cAMP/PKA., Biochim Biophys Acta 1692 (2004) 159-174.
[45] G. G. Cadd, M. D. Uhler and G. S. McKnight, Holoenzymes of cAMP-dependent protein kinase containing the neural form of type I regulatory subunit have an increased sensitivity to cyclic nucleotides., J Biol Chem 265 (1990) 19502-19506.
[46] A. B. Malmberg, E. P. Brandon, R. L. Idzerda, H. Liu, G. S. McKnight and A. I. Basbaum, Diminished inflammation and nociceptive pain with preservation of neuropathic pain in mice with a targeted mutation of the type I regulatory subunit of cAMP-dependent protein kinase., J Neurosci 17 (1997) 7462-7470.
[47] I. U. Khan, D. Laxminarayana and G. M. Kammer, Protein kinase A RI beta subunit deficiency in lupus T lymphocytes: bypassing a block in RI beta translation reconstitutes protein kinase A activity and augments IL-2 production., J Immunol 166 (2001) 7600-7605.

Figure Legends

Figure 1. Effect of pro-atherogenic cytokines on VSMC morphology as a function of cytoskeletal organization. A. Phase-contrast microscopy of cell morphology 12, and 72 h after stimulation with 5 ng/ml IL-1β, 10 ng/ml TNFα or 10 ng/ml IFNγ. **B.** Immunostaining for filamentous actin (F-actin) and vinculin 72 h after the treatment of PFA-fixed VSMCs, with Alexa Fluor 594-conjugated phalloidin (red) and FITC-coupled monoclonal anti-vinculin antibody (green) visualized by fluorescence microscopy. The images shown are representative of at least 3 independent experiments.

Figure 2. Effect of pro-atherogenic cytokines on the phosphorylation level of PKA substrates. A. Western-blot analysis of PKA substrate phosphorylation with β-actin as a loading control (**left panel**). Western-blot quantification for phosphorylated PKA substrates (**right panel**). The data shown are the means ± SEM of 5 independent experiments. *, $P < 0.05$, versus vehicle-treated cells in a Kruskal-Wallis test followed by Dunn's multiple comparison test.

Figure 3. IL-1β, TNFα and IFNγ do not increase intracellular cAMP concentration in an acute manner. Changes in intracellular [cAMP] were measured with the $^{T}Epac^{VV}$ biosensor, by wide-field fluorescence imaging on untreated VSMCs. Drugs were added to the bath for the period indicated by the bar on the graph: 10 μM isoproterenol (positive control, A), 5 ng/ml IL-1β (**B**), 10 ng/ml TNFα (**C**) or 10 ng/ml IFNγ (**D**). **Left panels.** Microscopy fields shown in black and white (**upper left**) are representative of fluorescence emission at 535 nm. The ratio was determined over individual cells within regions of interest (ROI) delimited with colored contours. The F480/F535 ratio, indicative of biosensor activation, was calculated for each pixel in the whole image. Pseudocolored images representing the F480/F535 emission ratio provide an indication of intracellular [cAMP] (**a**) before treatment, (**b**) during cytokins treatments and (**c**), with 10 μM forskolin + 200 μM IBMX, to maximize biosensor levels. The calibration square (**top right**) indicates fluorescence intensity (in counts/pixel/s) horizontally and F480/F535 ratio vertically. **Right panels.** Time course of F480/F535 ratio measurements averaged over individual ROIs. Each trace indicates F480/F535 emission ratio measurements for individual cells over time, corresponding to the ROI delimiting each cell. Gray traces

correspond to the F480/F535 emission ratio of cells outside the displayed region. The average of all traces is plotted as a thick black line. The data and images shown are representative of 4 independent experiments.

Figure 4. Conditioned medium (CM) from IL-1β-treated cells increases cAMP concentration and induces a change in VSMC morphology

CM was collected after the treatment of VSMCs with vehicle, IL-1β (5 ng/ml), TNFα (10 ng/ml) or IFNγ (10 ng/ml) for 72 h. Recipient cells were allowed to undergo transdifferentiation under the same treatment conditions for 48 h and were then starved overnight. The data and images shown are representative of at least 3 independent experiments. **Left and middle panels.** Vehicle- **(A)**, IL-1β- (**B**), TNFα- (**C**) or IFNγ-treated VSMCs (**D**) were perfused with the corresponding conditioned medium for the time indicated by the horizontal bar on the graphs. **Left panels.** See figure 3, legend for the left panel. **Middle panels.** See figure 3, legend for the right panel. **Right panels.** Phase-contrast microscopy of the morphological phenotype of VSMCs induced by one hour of treatment with vehicle-CM, IL-1β-CM, TNFα-CM and IFNγ-CM.

Figure 5. Inflammatory secretome induced by IL-1β, TNFα and IFNγ. VSMCs were treated with vehicle, IL-1β (5 ng/ml), TNFα (10 ng/ml) or IFNγ (10 ng/ml). **Left panels A and B.** Levels of mRNA after 48 h of stimulation, expressed as fold-changes with respect to vehicle. The diagram is based on the data shown in table 3 (mean ± SEM of 8 independent experiments). **Right panels A and B.** Analysis of the cell medium 72 h after stimulation, in a membrane-based antibody array **(A)** and by ELISA **(B).** Data for the PGE_2 assay and inflammatory gene mRNA levels are presented as the mean ± SEM of 6 and 8 independent experiments respectively. **, $P < 0.01$ versus vehicle-treated cells in Kruskal-Wallis tests followed by Dunn's multiple comparison tests. The results of the cytokine array analysis are representative of 2 independent experiments.

Figure 6. Blocking EP4 receptors suppresses the response to conditioned medium from IL-1β-treated VSMCs (IL-1β-CM, A) and PGE2 (B).

Panels A and B. Intracellular [cAMP] in naive VSMCs treated with (**A**) IL-1β-CM or (**B**) 50 nM PGE_2. The various EP antagonists were added successively, as indicated in the figure. The antagonist concentrations were as follows, 280 nM for SC51322 (EP1), 6 nM for

L798,106 (EP3) and 26 nM for ONO AE3208 (EP4). The black line indicates the duration of treatment. See the legend to the right panel in Figure 3 for details. **Panels C and D**. Quantification of the changes in cAMP concentration induced by (**C**) IL-1β-CM or (**D**) 50 nM PGE_2 in the presence or absence of the EP antagonists. n.s., non-significant, ***, $P < 0.001$ versus vehicle-treated cells in Kruskal-Wallis tests followed by Dunn's multiple comparison tests. **Panels E and F**. Phase-contrast microscopy of the changes in VSMC morphology induced by (**E**) IL-1β-CM or (**F**) 50 nM PGE_2 in the presence or absence of the EP antagonists. The data and images shown are representative of 3 independent experiments.

Figure 7. Role of PKA in the development of a stellate morphology in VSMCs

Phase-contrast microscopy of naive (**A**) and IL-1β-transdifferentiated (**B)** VSMCs in the presence of vehicle, Epac (8-pCPT-O-Me-cAMP, 100 µM) and/or PKA (6BNZ-cAMP, 100 µM) activators. The concentrations used for each compound are indicated on the figure. The results shown are representative of at least 3 independent experiments. **C**. Numbers of copies of PKA regulatory and catalytic subunit mRNAs in VSMCs treated with vehicle or IL-1β (5 ng/ml) for 48 h. The data shown are the means ± SEM of at least 4 independent experiments. *, $P < 0.05$, ***, $P < 0.001$ versus vehicle-treated cells in Kruskal-Wallis tests followed by Dunn's multiple comparison test. **D.** Phase-contrast microscopy of VSMCs transfected with control siRNA (siCTRL) or siRNA directed against the PKAR1α (siR1α) or PKAR1β (siR1β) subunits. **Upper and lower panels:** vehicle- and PGE_2-treated cells (50 nM for 1 hour), respectively.

Table

Table 1: Summary of qPCR primer sequences

Gene family	Target genes	Forward primers (5'-3')	Reverse primers (5'-3')	Accession numbers
Eicosanoids	COX-2	ggaagtctttggtctggtg	tcttgatcgtctctcctatcagta	NM_017232.3
	sPLA2 IIA	atggcctttggctcaat	gcaaccgtagaagccata	NM_031598.3
	PTGES	agctaggtgtgtggatctc	acaatcttctgtcctttgctttat	NM_021583.3
Chemokines	CXCL1	gactccagccacactccaac	cagcgctgcacagagaag	NM_030845.1
	CXCL2	ggatcgtccaaaagatactgaac	ggtacaggagcccatgttctt	NM_053647.1
	CXCL3	ggctcctcaatgctgcac	ggccacaacagtccctga	NM_138522.1
	CXCL5	cactgccacagcatcgag	ttaagcaaacacagcgtagctc	NM_022214.1
	CXCL10	atgaacccaagtgctgctgt	gtctcagcgtctgttcatgg	NM_139089.1
	CX3CL1	cgtgccacaagatgacctc	ctgtgctgtctcgtctccag	NM_134455.1
	CCL2	agcatccacgtgctgtctc	gatcatcttgccagtgaatgag	NM_031530.1
	CCL3	gcgctctggaacgaagtct	gaatttgccgtccataggag	NM_013025.2
	CCL20	ggggtactgctggcttacct	ggcagcagtcaaagttgctt	NM_019233.1
	GM-CSF	catctctaatgagttctccatccag	cccgtagaccctgcttgtat	NM_053852.1
	VEGF-A	ctatgtgctggctttggt	gagatagagtatatcttcaagccg	NM_001287108.1
Interleukins	IL6	tggtcttctggagttccg	agatatgaactagggtttcagtattg	NM_012589.2
Contractile markers	Calponin	cagccaggctggcatga	ccatctgcaagctgacg	NM_031747.1
	SM22-α	tatggcagcagtgcagag	ctttcttcataaaccagttggga	NM_031549.2
	Smoothelin	gcagtatgaagactacatttaccattg	tcagttctgctctctgttg	NM_001013049.2
	SM-MHC	tgagaggaagaagatggctca	tgtagtttctgtctggcagctt	NM_001170600.1
PKA subunits	PRKACA	cggggtcctcatctacga	tgaagtgggatgggaacc	NM_001100922.1
	PRKACB	gagtacctggccccagagat	ccaccagtccactgccttat	NM_001077645.1
	PRKAR1A	caataatgaatgggcaacca	atcaaagccagctctccaaa	NM_013181.1
	PRKAR1B	gatcccccaacgaggagtat	gcagggcaatctctccaa	NM_001033679.1
	PRKAR2A	tggatgtgatcggggaaa	aagctgtcggccttttca	NM_019264.2
	PRKAR2B	gtgctctgtggggtttgg	ttcctctttttggcattgtttt	NM_001030020.1
Housekeeping gene	Cyclophilin A	tgctggaccaaacacaaatg	cttcccaaagaccacatgct	NM_017101.1

Table 2: Amplitude of the dynamic cAMP response triggered by cytokine-treated VSMC conditioned medium. The amplitude of the response is indicated by the mean for the % of the maximum response (Rmax) obtained adding 10 µM forskolin + 200 µM IBMX. The data presented are the means ± SEM of 4 independent experiments on 10-30 individual cells per condition. Significance was evaluated in Kruskal-Wallis tests followed by Dunn's multiple comparison tests. **, $P < 0.01$ versus vehicle-treated cells.

Conditioned Medium (CM)	Mean (% of Rmax) ± SEM
Vehicle-CM	1.39 ± 0.76
IL-1β-CM	**34.5 ± 3.8****
TNFα-CM	3.80 ± 2.4 n.s
IFNγ-CM	2.37 ± 1.27 n.s

Table 3: Levels of mRNAs encoding inflammatory markers in transdifferentiated VSMCs. Confluent rat VSMCs were serum-starved and treated with vehicle, IL-1β (5 ng/ml), TNFα (10 ng/ml) or IFNγ (10 ng/ml). Relative levels of mRNAs encoding inflammatory markers, 48 h after stimulation, expressed as a fold-change with respect to vehicle. The results were first normalized with respect to cyclophilin A (PPIA) and the data shown are the mean value ± SEM of 7 or 8 independent experiments. Differences between groups were evaluated in Kruskal-Wallis tests followed by Dunn's multiple comparison tests. *, $P < 0.05$, **, $P < 0.01$ and ***, $P < 0.001$ versus vehicle-treated cells.

		Fold-change with respect to vehicle			
Gene Family	**Genes**	**Vehicle**	**IL-1β**	**TNFα**	**IFNγ**
Eicosanoid metabolism	COX-2	1.32 ± 0.38	175 ± 77 ***	1.4 ± 0.3 n.s	1.5 ± 0.3 n.s
	sPLA2 IIA	1.30 ± 0.36	33579 ± 6858 ***	4197 ± 1445 **	405 ± 271 n.s
	PTGES1	1.09 ± 0.18	1399 ± 359 ***	15.18 ± 3.95 *	3.96 ± 1.57 n.s
Cytokines / Chemokines	CXCL1	1.63 ± 0.6	859 ± 210 ***	63.4 ± 9.4 *	25.5 ± 12.4 n.s
	CXCL2	1.95 ± 0.89	17862 ± 8768 ***	326.2 ± 130 ***	9.18 ± 2.88 n.s
	CXCL3	1.08 ± 0.15	20027 ± 7272 ***	546 ± 98 *	36.5 ± 23.2 n.s
	CXCL5	2.18 ± 1.11	18572 ± 3777 ***	1162 ± 204 *	30.24 ± 9.06 n.s
	CXCL10	1.19 ± 0.27	9.34 ± 2.62 n.s	30.48 ± 3.49 *	5007 ± 974 ***
	CX3CL1	1.19 ± 0.22	70.98 ± 14.72 ***	42.1 ± 3.45 **	22.24 ± 6.25 n.s
	CCL2	1.07 ± 0.17	289 ± 38 ***	131 ± 7 **	32.2 ± 9.8 n.s
	CCL3	1.01 ± 0.09	1744.36 ± 632.6 ***	1.30 ± 0.17 n.s	2.12 ± 0.75 n.s
	CCL5	1.19 ± 0.28	3498 ± 1577 **	21337 ± 5183 ***	606 ± 191 n.s
	CCL20	1.33 ± 0.53	5915 ± 1123 ***	569 ± 105 **	62.44 ± 38.5 n.s
	GM-CSF	1.02 ± 0.08	11029 ± 2598 ***	67.00 ± 7.7 *	2.61 ± 0.81 n.s
	IL6	1.14 ± 0.18	1043 ± 143 ***	19.26 ± 3.16 *	7.32 ± 2.92 n.s
	VEGF-A	1.10 ± 0.18	4.02 ± 0.96 **	1.44 ± 0.16 n.s	1.53 ± 0.19 n.s

Figure 1

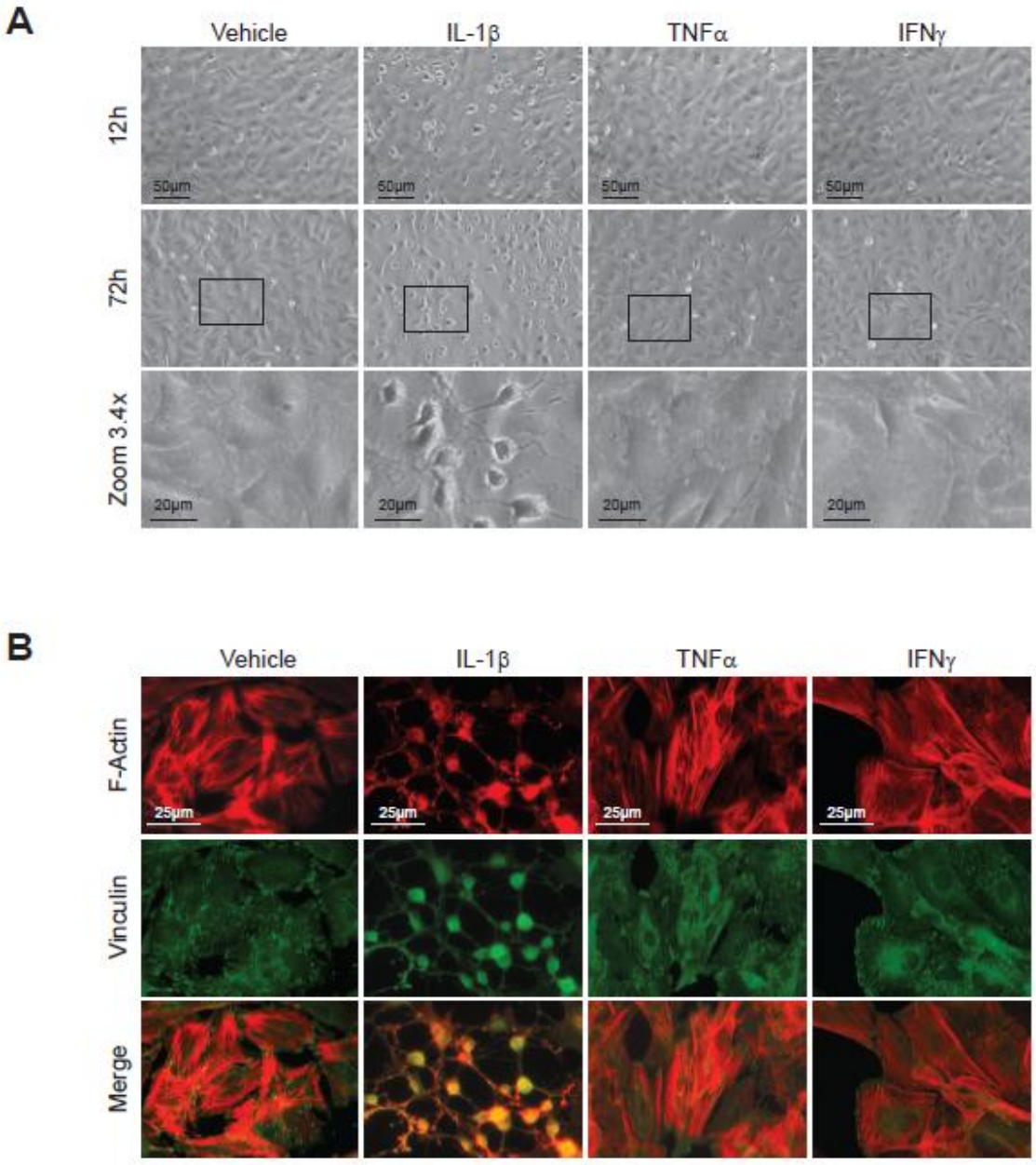

Figure 2

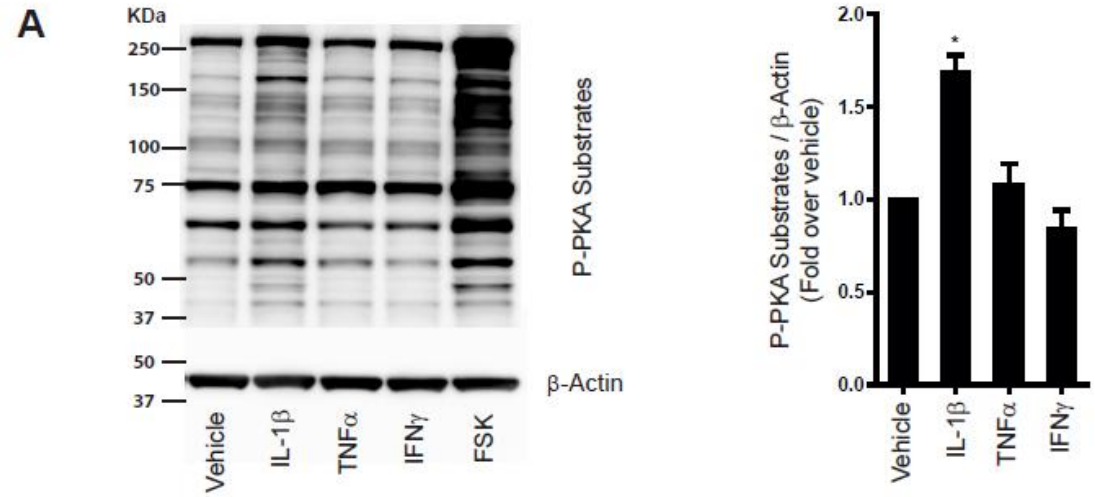

Figure 3

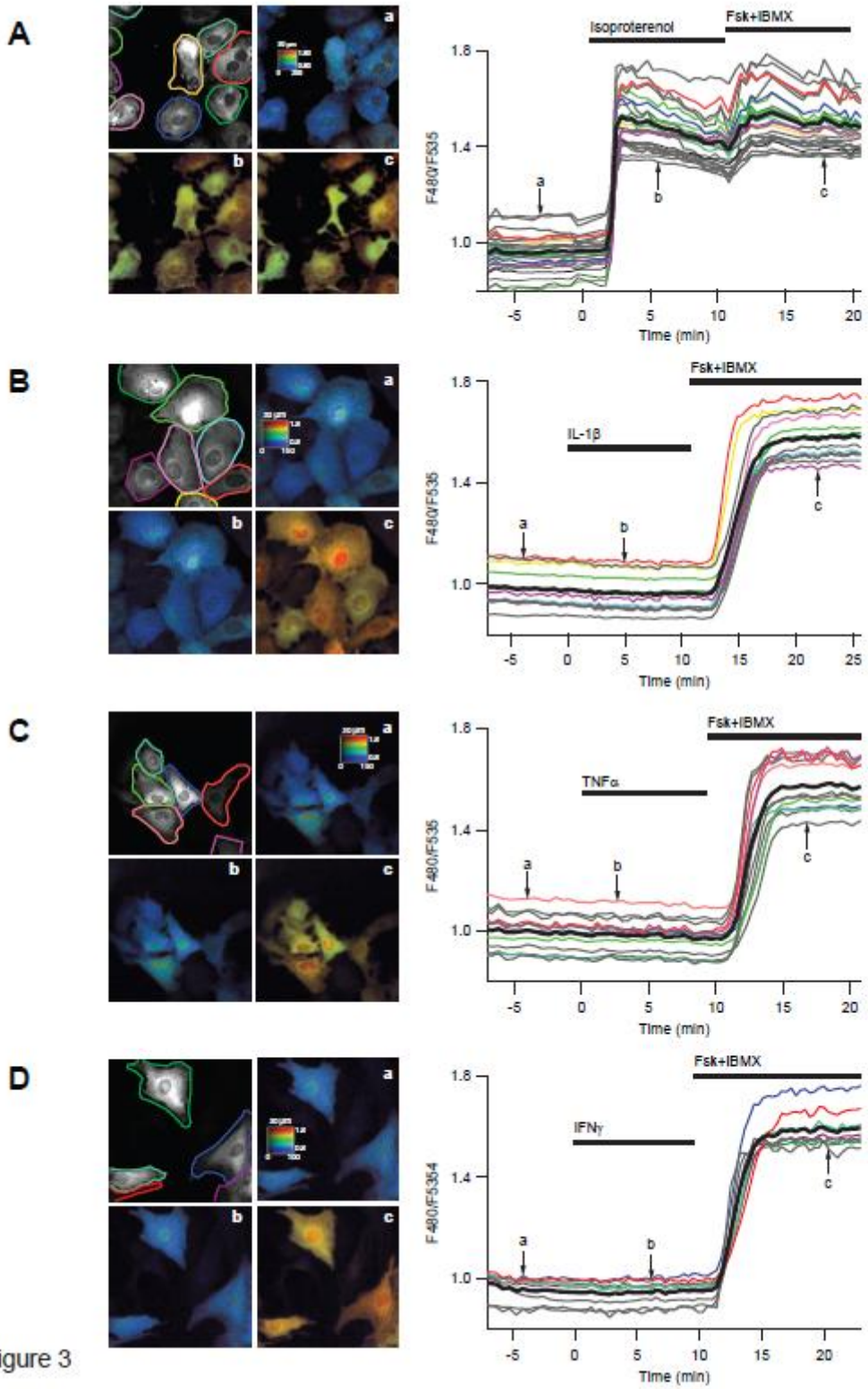

Figure 3

Figure 4

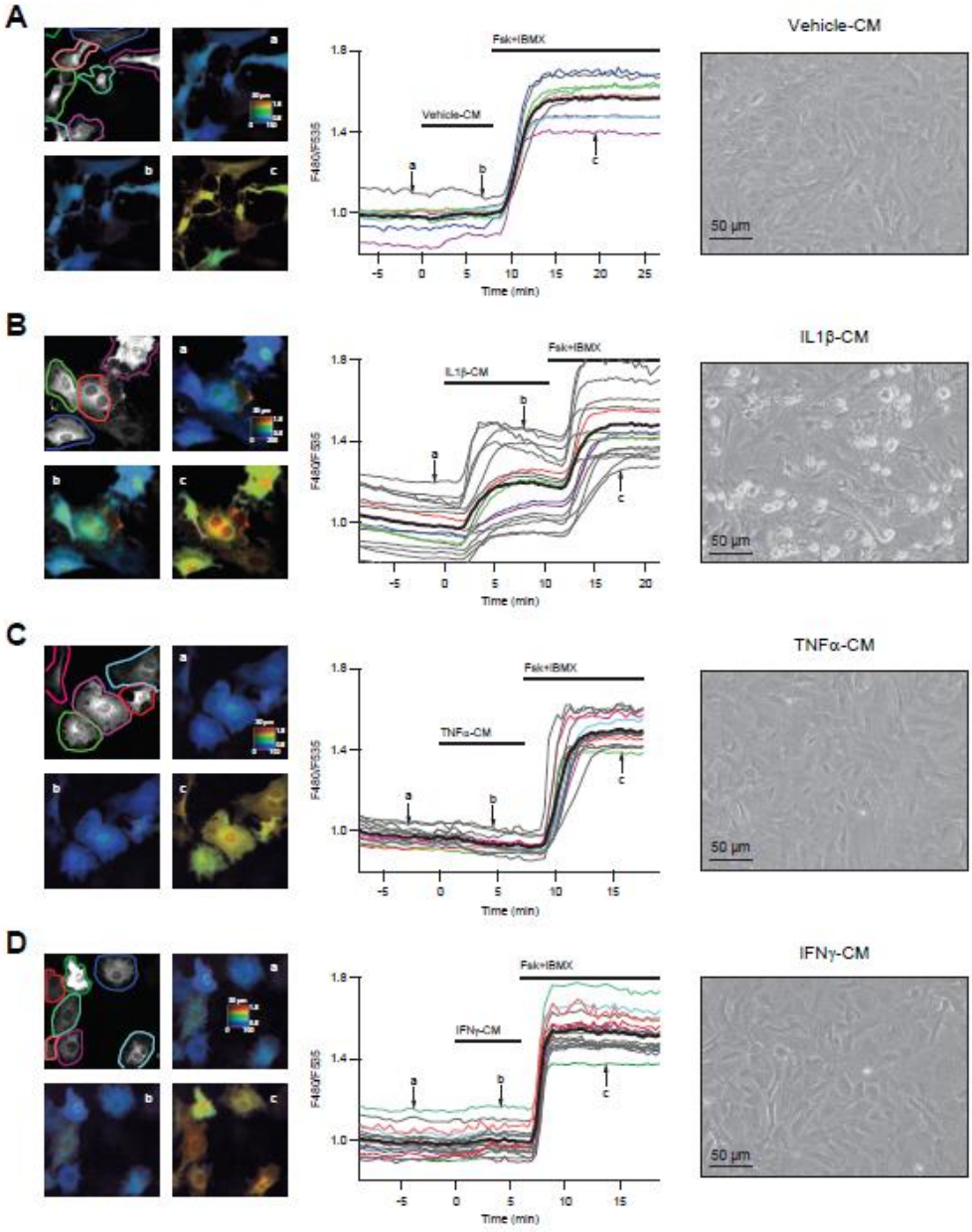

Figure 4

Figure 5

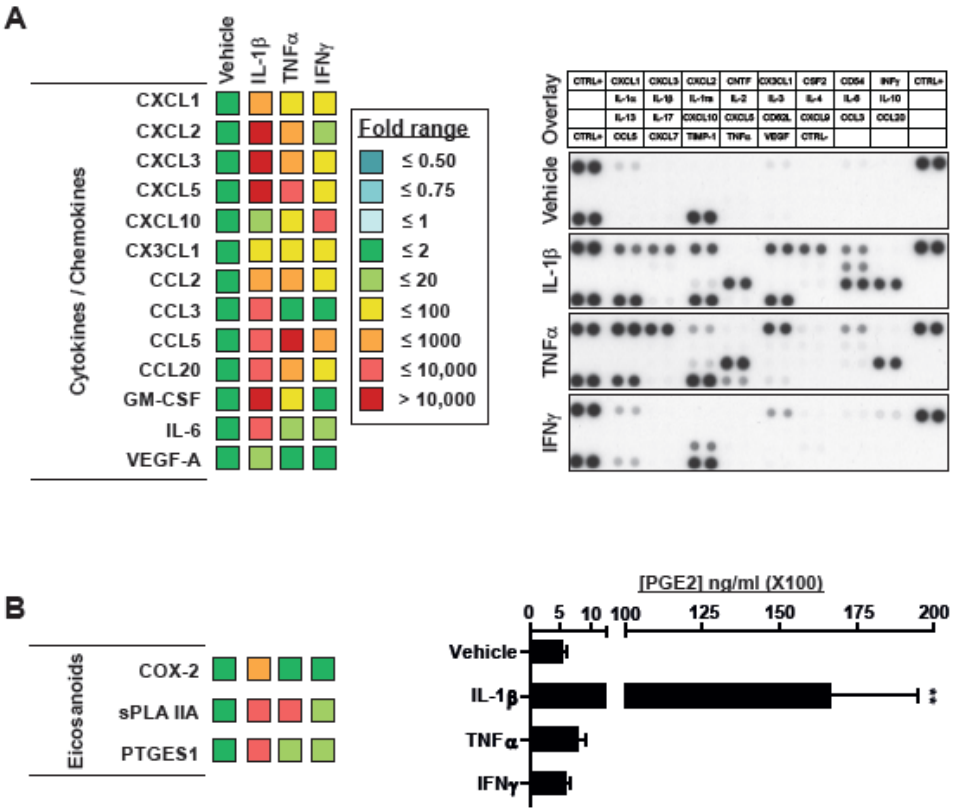

Figure 6

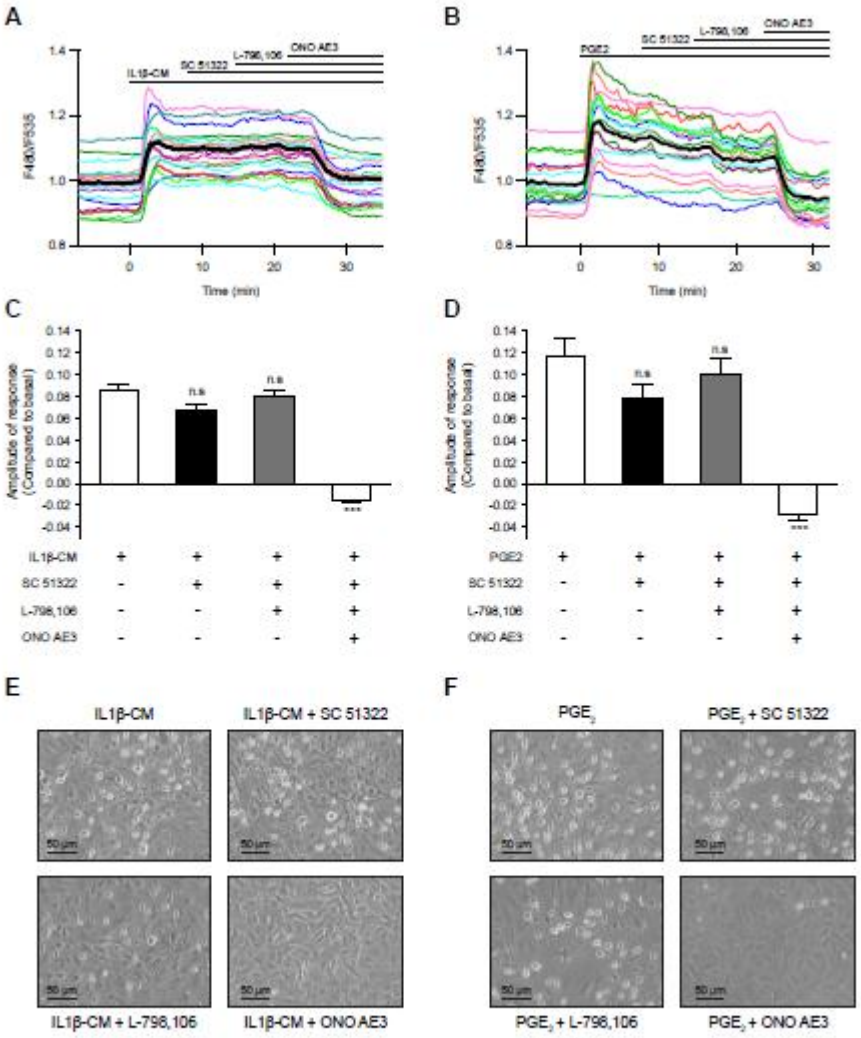

Figure 6

Figure 7

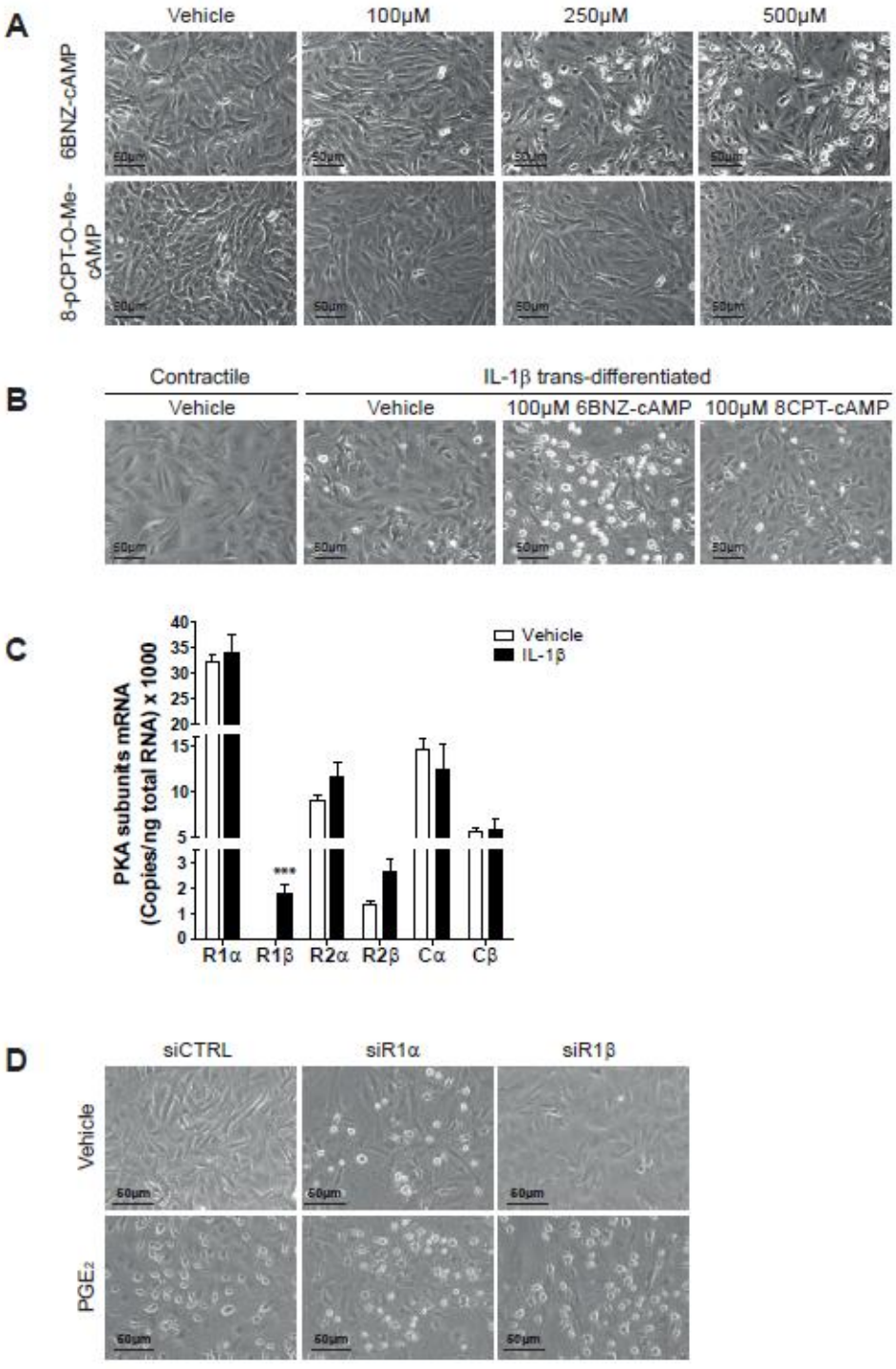

Figure 7

Highlights

- VSMCs transit from a contractile to a stellate morphology upon IL-1β stimulation.
- The IL-1β effect on VSMCs morphology is indirect and due to the secretion of the PGE_2.
- Binding to EP4, PGE_2 stimulates cAMP production and PKA, modifying cell structure.
- Silencing PKAR1α -but not R1β- mimicked the effect of IL-1β/PGE_2 on cell morphology.